ESTIMATING ECONOMIC LOSSES OF RC WALL BUILDINGS IN SEDIMENTARY BASINS BY COMBINING EMPIRICAL AND SIMULATED SEISMIC HAZARD CHARACTERIZATIONS

C. Molina Hutt[1], P. Kourehpaz[2], N. Marafi[3], J. Berman[4] and M. Eberhard[5]

[1] *Assistant Professor, Department of Civil Engineering, University of British Columbia, Vancouver, BC.*
carlos.molinahutt@civil.ubc.ca
[2] *PhD Student, Department of Civil Engineering, University of British Columbia, Vancouver, BC.*
pouriak@mail.ubc.ca
[3] Senior Modeler, Risk Management Solutions, Inc., Newark, CA.
marafi@uw.edu
[4] *Professor, Department of Civil & Environmental Engineering, University of Washington, Seattle, WA.*
jwberman@uw.edu
[5] *Professor, Department of Civil & Environmental Engineering, University of Washington, Seattle, WA.*
eberhard@uw.edu

Abstract

Studies of recorded ground motions and simulations have shown that deep sedimentary basins can greatly increase the intensity of earthquake ground motions at medium and long periods, i.e. 1-4 s. While future earthquake design provisions are likely to account for basin amplification, the consequences of accounting for these effects are uncertain. By combining empirical and simulated seismic hazard characterizations that account for the effects of basins, this paper estimates key indicators of seismic performance, expressed in terms of earthquake-induced repair costs, for a series of 12-story reinforced concrete shear wall archetype buildings in Seattle, WA. The reference archetype is designed to comply with ASCE 7-16 minimum design requirements, which neglect basin effects. A series of code-prescriptive design enhancements, five in total, are also evaluated. The enhancements include: (a) increasing design forces, (b) decreasing in drift limits, and (c) a combination of these strategies. As an additional reference point, a performance-based design is also assessed. The performance of the archetype buildings is evaluated for the seismic hazard level in Seattle according to the 2018 National Seismic Hazard Model (2018 NSHM), which explicitly considers basin effects. Increasing design forces by 25% combined with a reduction in drift limits to 1.5% was found to be the most efficient of the seven design strategies considered, resulting in a 51% reduction in the average annual losses compared to the reference archetype. Incorporating physics-based ground motion simulations to represent the large-magnitude Cascadia subduction interface earthquake contribution to the hazard results in an average increase in annual losses of 28% compared to the 2018 NSHM.

Keywords: Cascadia subduction zone, simulated ground motions, deep sedimentary basin effects, reinforced concrete shear walls, earthquake-induced losses.

1. INTRODUCTION

The Pacific Northwest has the potential to experience large-magnitude earthquakes generated by the Cascadia Subduction Zone (CSZ), which is located approximately 100 km from the city of Seattle. Furthermore, the city lies above a deep sedimentary basin, which can amplify the intensity of earthquake ground motions [1–3]. Current seismic design provisions in the US, i.e. ASCE 7-16 [4], were developed according to the 2014 National Seismic Hazard Model (NSHM) [5], which neglects basin effects. While future earthquake design provisions are likely to account for basin amplification, the consequences of accounting for these effects are uncertain.

Reinforced Concrete (RC) shear walls are commonly used in the western United States as the seismic force-resisting system in mid- to high-rise residential buildings [6]. Recent earthquakes, including the 2010 Maule earthquake (Chile) and the 2011 Christchurch earthquake (New Zealand), have demonstrated that modern RC shear wall buildings generally behave well in terms of life safety [7]. However, due to significant damage levels, post-earthquake repair of these buildings is costly and time consuming, leading to a long-lasting loss of occupancy and a slow recovery of the community.

In this paper, the anticipated seismic performance, expressed in terms of earthquake-induced repair costs, for range of 12-story RC shear wall buildings in Seattle was assessed. A reference archetype designed to comply with minimum ASCE 7-16 [4] code-prescriptive requirements was evaluated. A series of code-prescriptive design enhancements, five in total, were also studied. The enhancements included: (a) increasing design forces, (b) decreasing drift limits, and (c) a combination of these strategies. Lastly, an archetype designed following a performance-based approach [8] was also evaluated. The archetype buildings were designed by Marafi et al. [9] to quantify the impact of basin amplification on collapse risk and to devise simple design strategies to satisfy the 1% in 50-year collapse risk target of modern building codes when basin effects are considered.

The performance of the archetype buildings was evaluated for the seismic hazard level in Seattle according to the 2014 NSHM as well as the 2018 NSHM, which explicitly considers basin effects [10]. The archetype buildings were also subjected to 30 simulated scenarios of a magnitude-9 (M9) CSZ interface earthquake, recently generated by Frankel et al. [11]. These simulated ground motions were used to devise a hybrid seismic hazard model, which is based on the 2018 NSHM, but utilizes physics-based simulations to represent the large interface earthquake portion of the hazard and empirical relationships for all other earthquake sources (crustal and intraslab).

Numerous studies have quantified the earthquake-induced economic losses of modern and existing frame buildings. For instance, Hwang and Lignos [12] evaluated the seismic performance of modern steel moment-resisting frames, whereas Molina Hutt et al. [13–15] evaluated the performance of pre-Northridge steel moment frames. The performance of modern code-conforming [16] and non-ductile [17] RC moment frames has also been widely studied. However, analytical studies on the earthquake-induced repair costs of RC shear wall buildings remain limited. In addition to addressing this knowledge gap, this study quantifies the impact of basin amplification and variations in strength and stiffness on the earthquake-induced repair costs of RC shear wall buildings in Seattle.

2. CONSIDERING DEEP SEDIMENTARY BASINS IN STRUCTURAL DESIGN

Past studies have shown that recorded motions have spectral accelerations that are larger in deep sedimentary basins than in surrounding locations [1–3,18]. The effects of deep sedimentary basins on ground-motion characteristics have also been observed in physics-based simulations of earthquake ground motions [11,19–22]. In the United States, currently enforced seismic design provisions, i.e. ASCE 7-16, utilize spectral accelerations for use in design based on the 2014 NSHM, which does not consider basin amplification. In the western United States, deep basins underlie large metropolitan areas, including Seattle, San Francisco, Los Angeles and Salt Lake City. As a result, the most recent version of the national seismic hazard model, the 2018 NSHM, accounts for basin amplification on spectral accelerations in these areas and its adoption in future design standards would result in a considerable increase in seismic design spectral accelerations.

The 2018 NSHM accounts for basin effects on spectral acceleration for all earthquake sources using basin terms adapted from the crustal earthquake ground-motion models in the NGA West2 project [18]. The proxy for basin depth is the depth from the surface to a layer with a shear-wave velocity of at least 1.0 km/s or 2.5 km/s, denoted as $Z_{1.0}$ and $Z_{2.5}$, respectively. Compared to the other basins in the western United States, Seattle has the largest values of $Z_{2.5}$, which is equal to 6.9 km [23]. As a result, the increase in spectral accelerations from the 2014 to the 2018 NSHM Uniform Hazard Spectrum (UHS) for a hazard level with a 2% probability of exceedance in 50-year is approximately 50% for periods in the range of 1-4 s.

While the basin amplification terms used in the 2018 NSHM were developed by considering crustal earthquakes, interface earthquakes represent the largest contribution to the seismic hazard in Seattle, particularly at periods greater than 1 s. Comparing response spectra developed per the 2018 NSHM and M9 simulations revealed that 2018 NSHM underestimated the basin effect on spectral acceleration at periods longer than 1 second in the Seattle area [11,24].

Recent studies have evaluated the impact of basin amplification on collapse risk. Marafi et al. [9] found that the collapse risk of modern RC shear wall buildings in Seattle would increase from 0.5% to 1.3% in 50-years when basin effects are considered. Similarly, Molina Hutt et al. [15] found that the 50-year collapse risk of 1970s steel moment frames would increase from 6.9% to 10.5%. However, the impact of basin amplification on earthquake-induced repair costs has not yet been quantified.

3. ARCHETYPE RC SHEAR WALL BUILDINGS

We studied the seismic performance of seven design variations of a 12-story residential RC shear wall building in Seattle, as summarized in Table 1. All buildings were designed and detailed by Marafi et al. [9] as special RC shear walls (Chapter 18 of ACI 318-14 [25]), with a seismic force-reduction factor (R) of 6, following a modal response spectrum analysis (MRSA) procedure. The reference (REF) archetype was designed to barely meet the minimum code-prescriptive requirements of ASCE 7-16, with a 2% maximum allowable seismic drift, and a 1.0 flexural demand-to-capacity ratio at the ground floor. The REF archetype was also re-designed with an increase in design lateral loads of 25% and 50% (S25% and S50%, respectively). The REF archetype was also re-desined with a reduction in drift limits from 2% to 1.5% and 1.25% (DL1.5% and DL1.25%, respectively). Lastly, the REF archetype was re-designed by combining a 25% increase in design lateral loads and a reduction in drift limits of 1.5% (S25%+DL1.5%). In addition to the code-prescriptive designs, one additional design strategy followed a performance-based approach (PBD), which included nonlinear analysis to check the strain, force, and drift limits of the Tall Building Initiative (TBI) guidelines [26] as outlined in Seattle's Director's Rule 5 [8].

Table 1. Design strategies of the 12-story residential RC shear wall archetype buildings.

Design Strategy	Description
REF	Reference archetype designed per ASCE 7-16 (2% drift limit)
S25%	REF archetype redesigned with 25% increase in design lateral loads
S50%	REF archetype redesigned with 50% increase in design lateral loads
DL1.5%	REF archetype redesigned to meet 1.5% drift limit
DL1.25%	REF archetype redesigned to meet 1.25% drift limit
S25%+DL1.5%	REF archetype redesigned with 25% increase in design lateral loads and 1.5% drift limit
PBD	Performance-Based Design

The concrete compressive strength of RC shear walls was 55.2 MPa (8 ksi) and steel reinforcing had nominal yield strength of 414 MPa (60 ksi). For all 12-story archetypes, the floor dimensions were 48.8 m long by 48.8 m wide (160 ft x 160 ft) in basement levels and 30.5 m long by 30.5 m wide (100 ft x 100 ft)

above grade. The height for all stories including basement levels was 3.05 m (10 ft). Fig. 1 depicts the average, across all stories, RC shear wall and longitudinal steel reinforcement areas normalized by the total floor area. These metrics highlight how all design variations utilize a larger volume of concrete than the REF archetype. The S50% archetype results in the largest increase, with around 50% greater RC shear wall area over total floor area. The steel tonnage fluctuates across designs, with the S50% archetype utilizing 65% more steel than the REF archetype, and the DL1.25% design utilizes roughly 60% of the REF archetype. Additional details of the RC shear wall building designs can be found in Marafi et al. [9].
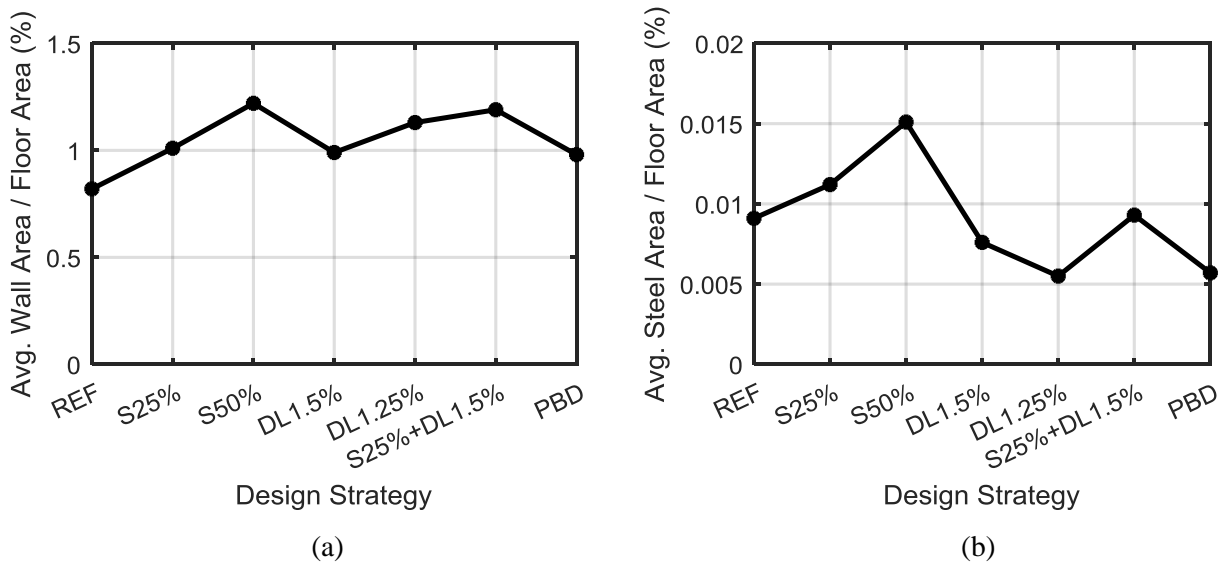

| (a) | (b) |

Figure 1. Variation of material quantities for different design strategies: (a) average RC shear wall area as percentage of floor area, and (b) average longitudinal steel reinforcement area as percentage of floor area.

4. SEISMIC PERFORMANCE ASSESSMENT METHODOLOGY

4.1. Seismic Hazard and Ground Motions

The seismic performance of each archetype building was evaluated using a multiple stripe analysis (MSA) procedure [27] consistent with that outlined in Marafi et al. [9]. In MSA, structural assessments are performed at a series of ground motion intensities spanning from high to low probability of occurrence. The lower- and upper-bound intensity measure levels considered cover a range from negligible damage to complete loss. Nonlinear dynamic analyses were conducted with ground motion suites representative of each intensity level. The analysis results were then linked back to probabilistic seismic hazard data, which enables calculating a range of risk metrics, such as annualized losses.

The intensity measure used in the MSA was the spectral acceleration at the fundamental period (T_1) of each archetype building. The MSA utilized median spectral acceleration over all orientations (SA_{RotD50}) to permit integration with probabilistic seismic hazard data. The intensity stripes used in the MSA had return periods of 100, 475, 975, 2475, and 4975-years. A Conditional Mean Spectrum (CMS) was used to represent the expected ground motion response spectrum conditioned on the occurrence of the target spectral acceleration at the fundamental period of each archetype. The CMS was calculated as a weighted average of the CMS for each ground-motion model and particular seismic source (e.g., Seattle fault) according to its percentage contribution to the hazard, as obtained by seismic hazard deaggregation results. For each return period, the CMS was computed using the 2014 and 2018 NSHMs [28] for the downtown Seattle location. At each return period, 100 ground motion records consisting of crustal, interface, and intraslab earthquakes were selected such that the ratio of each different earthquake type is proportional to its contribution to the total hazard. Ground motions were selected and scaled to match the target mean and variance Conditional Spectra (CS) [29].

The archetype buildings were also subjected to 30 sets of broadband seismograms for M9 CSZ earthquakes by combining synthetic seismograms derived from 3D finite-difference simulations ($\geq$ 1 s) with finite-source stochastic synthetics (<1 s), produced by Frankel et al. [11]. The resulting synthetics highlight considerable amplification of spectral accelerations, ranging from 2 to 5 between periods of 1 to 10 s, for sites within the Seattle basin.

4.2. Nonlinear Simulation of Structural Response

The structural response of all archetypes was evaluated by creating 2D nonlinear models in OpenSees. The axial and flexural nonlinear response of RC shear walls were captured by using displacement-based, beam-column elements with lumped-plasticity fiber sections [9]. The earthquake forces only applied in the uncoupled direction of the RC shear wall buildings, and therefore, effects of torsion and bidirectional loading on structural response were not taken into account. Nonlinear dynamic analysis were performed under 100 earthquake ground motion records at each intensity level for each archetype following the 2014 and 2018 NSHMs. Additionally, structural response was evaluated under thirty M9 CSZ earthquakes simulations. Fig. 2 illustrates the median peak story drifts and floor accelerations of each ground motion suite considered in the assessment of the REF archetype.
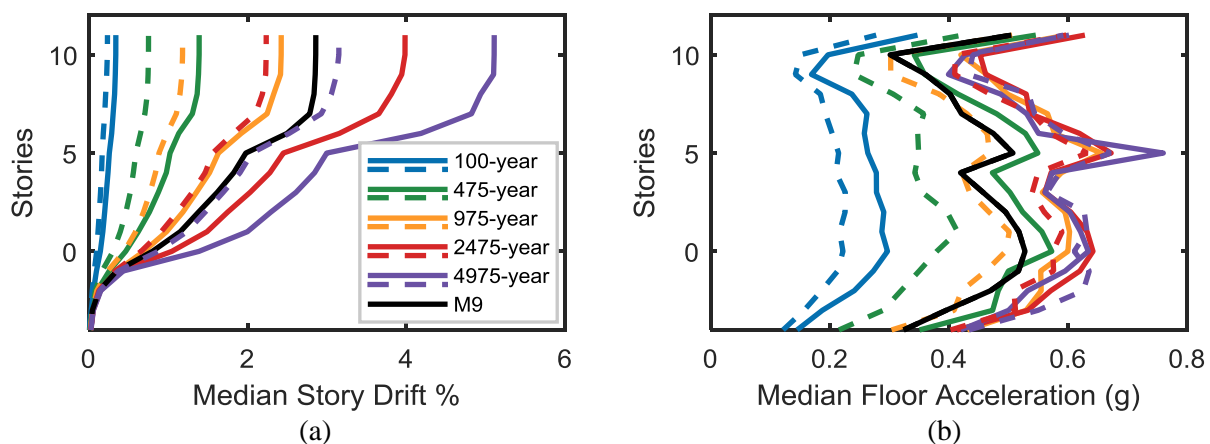

Figure 2. (a) Median story drift ratios and (b) median floor accelerations of the REF archetype, where solid lines correspond to the 2018 NSHM and dashed lines correspond to the 2014 NSHM.

In limited instances, at high earthquake shaking intensities, dynamic instability occurred when the lateral displacement of the structure increased without bounds. Additionally, non-simulated collapse modes were also considered in the assessment. Past experimental studies showed that probability of slab-column punching shear failure with respect to slab-column rotation depends on gravity shear ratio [30,31]. Available experimental data for slab-columns with shear-reinforcement and a gravity shear ratio between 0.4 to 0.6, permitted describing the slab-column rotation capacity data by means of a lognormal cumulative distribution with a mean of slab-column rotation of 5.9% and a dispersion of 0.12 [32–34]. In this study, non-simulated collapse was assumed to occur if slab-column rotation exceeded 5.9%.

Hazard consistent collapse fragilities were developed for all archetypes considering both simulated and non-simulated collapses. The probability of collapse at each return period was calculated by dividing number of collapse realizations over the total number of ground motions runs. A cumulative lognormal distribution was fitted to the data using a maximum likelihood estimation procedure, as outlined in Baker [35]. Fig. 3 shows the collapse fragilities of all archetype buildings considered in the assessment according to the 2018 NSHM, including only the interface earthquake contribution to the hazard, and the 2018 NSHM, including the contribution of all seismic sources to the hazard. Because each archetype has a unique fundamental period T_1, Fig. 3 shows the collapse fragilities with respect to return period of SA_{T1} to permit a visual comparison of all collapse fragilities. It can be observed that all design strategies considered result in a drastic reduction in the

probability of collapse with respect to the REF archetype. Furthermore, it should be noted that considering only the earthquake interface contribution to the hazard results in a reduced probability of collapse for any given return period because for a given spectral acceleration, the interface earthquake hazard is a fraction of total hazard, and therefore, the corresponding return period for a similar spectral acceleration is greater than the return period per the 2018 NSHM. Analysis of the archetype buildings with earthquake ground motion consistent with the 2014 NSHM resulted in a negligible probability of collapse.
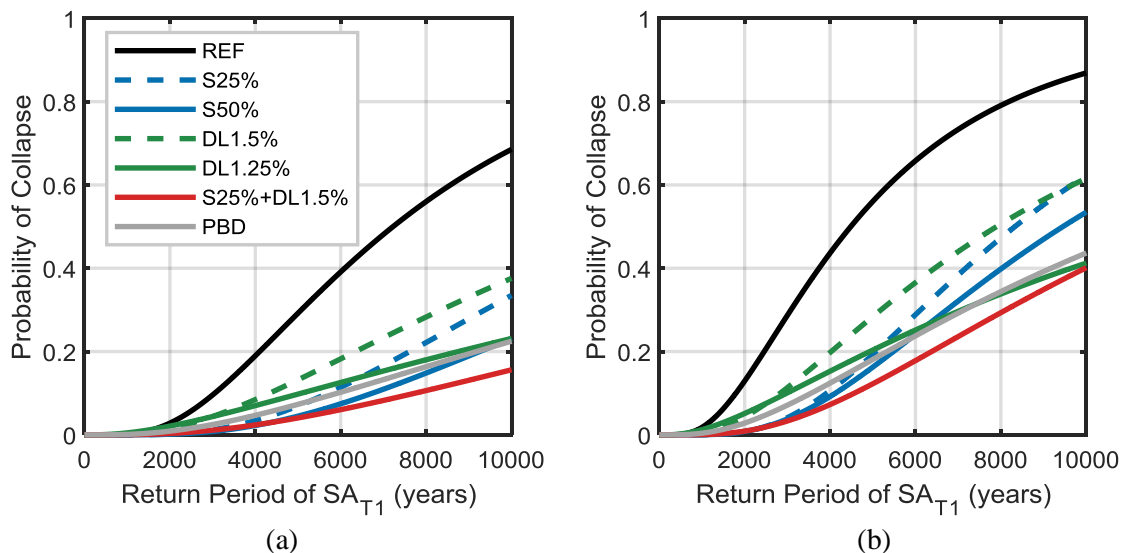

Figure 3. Collapse fragilities for the 12-story RC shear wall archetypes per (a) the 2018 NSHM, including only the interface earthquakes contribution to the hazard, and (b) the 2018 NSHM, including the contribution of all seismic sources to the hazard.

4.3. Loss Assessment

A risk-based assessment was carried out to calculate the average annual losses (AAL) of each archetype building. Additionally, the results were used to construct seismic vulnerability functions to permit rapid loss evaluations for regional and/or building portfolio risk assessments. A risk-based assessment consists of the evaluation of a number of intensity-based performance assessments under a range of ground motion intensity levels, five in this study, which are then combined with the ground motion hazard curve to provide the annual rates of exceedance of a performance measure, e.g. economic loss [36]. The technical basis of this methodology was developed by the Pacific Earthquake Engineering Research (PEER) center and applies the total probability theorem to predict earthquake consequences in terms of the probability of incurring a particular value of a performance measure [37]. Under this framework, performance is computed by integrating (1) the probability of incurring an earthquake of different intensities over all possible intensities, (2) the probability of incurring a certain building response (e.g. drift, acceleration, etc.) given an intensity of ground shaking, and (3) the probability of incurring certain damage and consequences given a value of building response [38].

The risk-based assessments were carried out consistent with the 2014 and 2018 NSHMs. Additionally, a scenario-based assessment was performed to evaluate the response of the archetype buildings conditioned on the occurrence of the M9 CSZ simulated earthquake scenarios. At each earthquake intensity level considered in the study, two thousand loss simulations were carried out. For each realization, the losses are calculated as follows: (i) engineering demand parameters, e.g. peak story drifts and accelerations (Fig. 2), are estimated from the results of nonlinear dynamic analyses; (ii) fragility functions are used in conjunction with engineering demand parameters to determine the associated damage state for each component (structural and non-structural); (iii) consequence functions are then used to translate damage states into repair costs [38]. The direct economic losses for each realization are then estimated by conducting this calculation for every

component at every story throughout the building. The loss assessment was carried out using SP3 [39], a software which implements the FEMA P-58 methodology [38].

A building performance model was created for each archetype building to enable its earthquake-induced repair costs. Table 2 summarizes the key assumptions of the building performance model, which apply to all archetypes, including location, design year, number of stories, occupancy, risk category, cost per square foot and total building square footage. The building replacement cost for the archetype residential building in Seattle was estimated by adjusting values recommended by FEMA P-58 for office buildings in California to account for differences in location [39] and occupancy type [40].

Table 2. Building Information.

Location	Lat., Long.	Design Year	Story Levels	Occupancy	Risk Category	Cost per sq. ft.	Total building sq. footage
Seattle, WA	47.6°N, -122.3°W	2019	12 (stories) +4 (basements)	Residential	II	$230	206800 ft²

Structural component quantities were based on the structural design of each archetype building, with slight variations depending on the design strategy. Non-structural component quantities were estimated based on typical quantities found in residential buildings using the FEMA P58 Normative Quantity Estimation Tool [38] and adjusted per the recommendations of USGS [41] and ATC [42]. Non-structural quantities were consistent for all building archetypes. A summary of the building performance model for all archetype buildings is documented in more detail in [43], including the structural and non-structural components adopted in each model, their fragility numbers (unique identifiers), component category (e.g. structure, façade, MEP, fitouts, etc.), engineering demand parameters, units, quantities and distribution of components throughout the building.

Different engineering demand parameters were used for different building components, depending on their ability to predict damage (e.g., damage to acceleration-sensitive components can be estimated by peak floor accelerations). The following demand parameters, derived from the nonlinear analysis results, were used to evaluate performance the archetype residential RC shear wall building: story drifts, residual drift, damageable wall drift, racking drift, and floor acceleration. Racking drift deformations occur in the RCSW structure due to differences in axial deformation (elongation) between the concrete walls and the gravity framing. The amplified racking causes damage and losses associated with interior partition wall finishes and slab-to-column connections. For the damage assessment of wall piers, simply using story drift ratio as a proxy for damage is not appropriate. For instance, on the upper floors of the archetype buildings, rigid body rotation contributes significantly to the story drifts. However, this mode of deformation does not cause damage to the wall piers. Therefore, damageable wall drifts, which remove the effect of rigid body rotation, were used as a better proxy for damage.

Residual drift was also included in the analysis to account for cases where the building is assumed to be damaged beyond repair. Residual drift is uncertain and highly sensitive to the nonlinear modeling assumptions and ground motion characteristics. Hence, residual drift was estimated as a function of peak story drift and yield drift following FEMA [38] recommendations. A building repair fragility, represented by a cumulative lognormal distribution with a median value of 1% residual drift ratio and a dispersion of 0.3, was assumed in the analysis.

5. INDICATORS OF SEISMIC PERFORMANCE

Vulnerability functions are powerful tools to estimate expected losses at different earthquake intensity measure levels. Fig. 4 shows the vulnerability functions, which describe the expected loss ratio as a function of the return period of SA_{T1} per the 2014 and 2018 NSHMs. The loss ratio is equal to the expected earthquake-induced repair costs, as determined from the loss assessment, normalized by the replacement value of the

building. As seen in Fig. 4, at any return period, expected losses per the 2018 NSHM are considerably higher than those of the 2014 NSHM for all archetypes considered in the assessment.

Past studies suggest that many owners may elect to replace buildings when the projected repair costs exceed about 40 to 50% of the replacement cost [38]. When basin effects are neglected, the REF archetype reached this threshold at a return period of approximately 2500 years. Consideration of basin effects lowered the return period of this critical loss threshold to less than 1000 years. However, adopting the S25%+DL1.5% design strategy would increase the return period back to 2500 years.
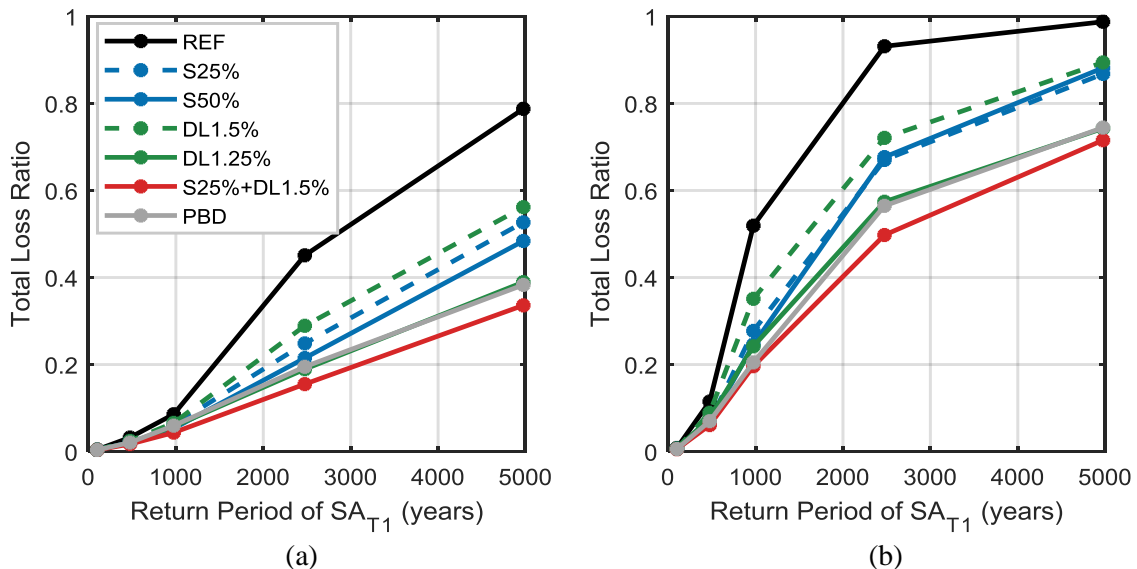

(a)   (b)

Figure 4. Loss vulnerability functions for 12-story archetypes per (a) the 2014 and (b) the 2018 NSHMs.

While vulnerability functions provide the loss values at various earthquake intensity measure levels, AAL is a useful metric to describe the anticipated economic losses considering damage at all earthquake shaking intensity levels, expressed in the form of an annualized payment. Hence, this metric can be regarded as a proxy for annual insurance payments. As illustrated in Fig. 5, consideration of basin effects resulted in a threefold increase in the AAL of the REF archetype from 0.06% to 0.16% of building replacement cost, which for the archetype building considered, is equivalent to $28000 and $76000 in annual losses, respectively.

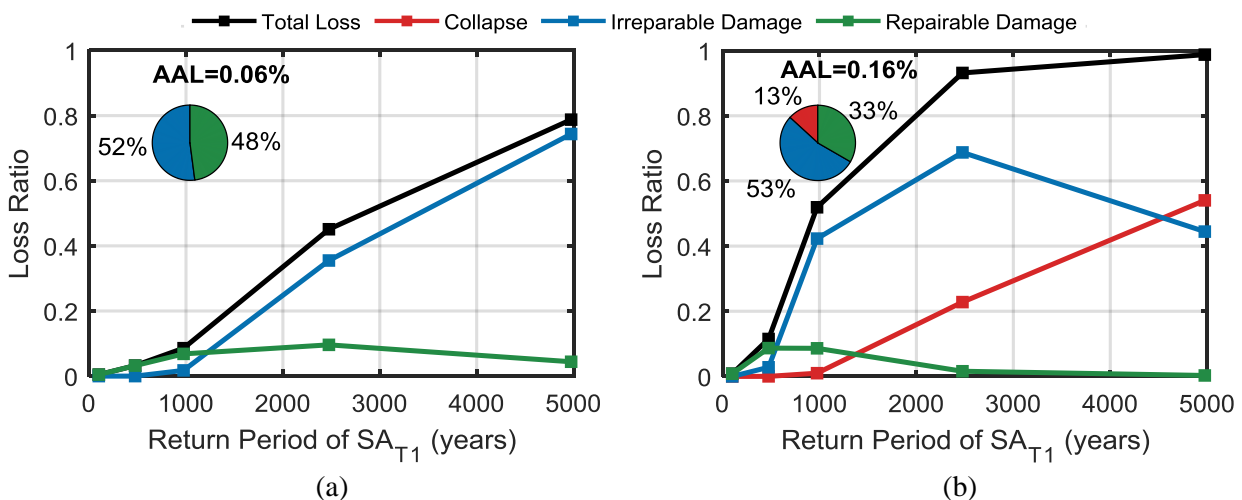(a)   (b)

Figure 5. Loss vulnerability functions and associated average annual loss (AAL) including contributions from collapse, irreparable and repairable damage for 12-story REF archetype per (a) the 2014 and (b) the 2018 NSHMs.

In estimating AALs, it is useful to deaggregate the loss in terms of its key contributors: (a) repairable damage, (b) irreparable damage due to excessive residual drifts (requiring demolition), and (c) collapse. Past studies [14,44] suggest that irreparable damage drives the AALs in modern buildings, whereas collapse drives the losses in older seismically vulnerable buildings. As illustrated in Fig. 5a, collapse contribution to AAL was negligible per the 2014 NSHM, highlighting the success of code provision in delivering low collapse risk (<1% in 50 years). However, consideration of basin effects resulted in unacceptable collapse risk and consequently considerable collapse contributions to AAL, 13% for the REF archetype, as seen in Fig. 5b.

Fig. 5 also illustrates the different loss contributions at each intensity level considered in the assessment. Regardless of the hazard model, at lower intensity levels (return period of 100 and 475 years) losses were driven by repairable damage, including structural and non-structural component damage. However, at higher hazard levels (return period greater than 2475 years per the 2014 NSHM and 1000 years per the 2018 NSHM) irreparable damage due to excessive residual drift became the greatest contributor to the loss, with the exception of the 4975-year hazard level per the 2018 NSHM, where collapse dominated the loss.

Fig. 6 summarizes the AAL for all design strategies considered computed using three distinct seismic hazard models: 2014 NSHM, 2018 NSMH and 2018 NSHM+M9. The latter represents a hybrid seismic hazard model, which is based on the 2018 NSHM, but utilizes physics-based simulations to represent the large interface earthquake portion of the hazard and empirical relationships for all other earthquake sources (crustal and intraslab). The hybrid seismic hazard model, permits calculating AALs as outlined in Eq. (1).

$$AAL_{NSHM\ 2018+M9} = AAL_{NSHM\ 2018} - AAL_{Interface} + AAL_{M9} \qquad (1)$$

Where, $AAL_{NSHM\ 2018+M9}$ is the total seismic loss including M9 interface earthquakes, $AAL_{NSHM\ 2018}$ is the seismic loss per 2018 NSHM, $AAL_{Interface}$ is the seismic loss for interface earthquakes only, and AAL_{M9} is the seismic loss corresponding to the M9 simulations.

Fig. 6 illustrates that the 2018 NSHM, i.e. consideration of basin effects, resulted in a threefold increase in AALs over the 2014 NSHM. Furthermore, using physics-based simulations to represent the large interface earthquake portion of the hazard resulted in a further increase of 28% over the 2018 NSHM losses. Fig. 6 also permits comparison of different design strategies. Regardless of the seismic hazard model considered, the results indicated that DL1.5% was the least effective strategy to reduce losses, achieving a 25% reduction over the REF archetype. Whereas the S25%+DL1.5% strategy was the most effective, achieving a 51% reduction in losses on average over the REF archetype. Increasing design strength from 25% to 50% had a minimal impact on AAL. On the other hand, reducing design drift limits to 1.25% had considerable impacts on reducing AALs.
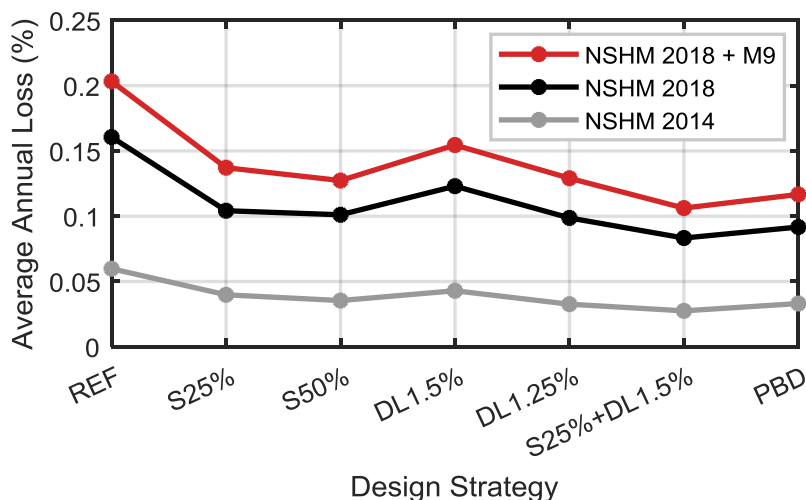

Figure 6. Average Annual Loss (AAL) for different design strategies and seismic hazard models.

6. CONCLUSIONS

This study quantified the earthquake-induced economic losses of a series of modern 12-story residential RC shear wall buildings in Seattle, with and without consideration of basin effects, as implemented in the 2018 and the 2014 NSHMs respectively. Furthermore, a hybrid hazard model was considered in the loss assessment to incorporate recent M9 CSZ earthquake simulations.

Expected losses were calculated at different intensity levels for all archetype buildings. Losses were then integrated with the corresponding seismic hazard curves to report AALs. Consideration of basin effects resulted in a threefold increase in AALs when basin effects were considered within the probabilistic seismic hazard assessment, i.e. the 2018 NSHM. Furthermore, consideration of physics-based simulations in the loss assessment resulted in a further increase of 28% over the 2018 NSHM estimates. Comparison of AALs across all design schemes considered revealed that the S25%+DL1.5% was the most effective and DL1.5% was the least effective design strategy to reduce annual losses relative to REF archetype, with 25% and 51% reduction in losses respectively.

7. ACKNOWLEDGEMENTS

8. REFERENCES

[1]   Morikawa, N. and Fujiwara, H. (2013) A new ground motion prediction equation for Japan applicable up to M9 mega-earthquake. *Journal of Disaster Research*. 8 (5), 877–888.

[2]   Choi, Y., Stewart, J.P., and Graves, R.W. (2005) Empirical model for basin effects accounts for basin depth and source location. *Bulletin of the Seismological Society of America*. 95 (4), 1412–1427.

[3]   Marafi, N.A., Eberhard, M.O., Berman, J.W., Wirth, E.A., and Frankel, A.D. (2017) Effects of deep basins on structural collapse during large subduction earthquakes. *Earthquake Spectra*. 33 (3), 963–997.

[4]   ASCE (2016) Minimum Design Loads for Buildings and Other Structures ASCE/SEI 7-16. American Society of Civil Engineers, Reston, VA.

[5]   Petersen, M.D., Moschetti, M.P., Powers, P.M., Mueller, C.S., Haller, K.M., Frankel, A.D., et al. (2014) Documentation for the 2014 Update of the United States National Seismic Hazard Maps. *U.S. Geological Survey Open-File Report*. 243 p.

[6]   Marafi, N.A., Ahmed, K.A., Lehman, D.E., and Lowes, L.N. (2019) Variability in seismic collapse probabilities of solid- and coupled-wall buildings. *Journal of Structural Engineering*. 145 (6), 1–17.

[7]   Ji, X., Liu, D., Ya, S., and Molina Hutt, C. (2017) Seismic performance assessment of a hybrid coupled wall system with replaceable steel coupling beams versus traditional RC coupling beams. *Earthquake Engineering & Structural Dynamics*. 46 (4), 517–535.

[8]   City of Seattle Department of Planning and Developments (2015) Alternate design requirements for use of special reinforced concrete shear walls in over height buildings. Retrieved April 21, 2018, from www.seattle.gov/dpd/codes/dr/DR2015-5.pdf.

[9]   Marafi, N.A., Makdisi, A.J., Berman, J.W., and Eberhard, M.O. (2020) Design strategies to achieve target collapse risks for RC-wall buildings in sedimentary basins. *Earthquake Spectra*. In Press.

[10]   USGS (2018) Preliminary 2018 update of the U.S. National Seismic Hazard Model: Overview of model, changes, and implications. United States Geological Survey. Retrieved from www.usgs.gov.

[11]   Frankel, A., Wirth, E., Marafi, N., Vidale, J., and Stephenson, W. (2018) Broadband synthetic seismograms for

magnitude 9 earthquakes on the cascadia megathrust based on 3D simulations and stochastic synthetics, Part 1: Methodology and overall results. *Bulletin of the Seismological Society of America*. 108 (5), 2347–2369.

[12] Hwang, S.H. and Lignos, D.G. (2017) Earthquake-induced loss assessment of steel frame buildings with special moment frames designed in highly seismic regions. *Earthquake Engineering and Structural Dynamics*. 46 (13), 2141–2162.

[13] Molina Hutt, C., Almufti, I., Willford, M., and Deierlein, G. (2016) Seismic loss and downtime assessment of existing tall steel-framed buildings and strategies for increased resilience. *Journal of Structural Engineering*. 142 (8), 1–17.

[14] Molina Hutt, C., Rossetto, T., and Deierlein, G.G. (2019) Comparative risk-based seismic assessment of 1970s vs modern tall steel moment frames. *Journal of Constructional Steel Research*. 159 598–610.

[15] Molina Hutt, C., Zahedimazandarani, S., Marafi, N.A., Berman, J.W., and Eberhard, M.O. (2020) Collapse risk of tall steel moment-resisting frames in deep sedimentary basins during large magnitude subduction earthquakes. *Engineering Structures, In-Review*.

[16] Ramirez, C.M., Liel, A.B., Mitrani-reiser, J., Haselton, C.B., Spear, A.D., Steiner, J., et al. (2012) Expected earthquake damage and repair costs in reinforced concrete frame buildings. *Earthquake Engineering & Structural Dynamics*. 41 (11), 1455–1475.

[17] Baradaran Shoraka, M., Yang, T.Y., and Elwood, K.J. (2013) Seismic loss estimation of non-ductile reinforced concrete buildings. *Earthquake Engineering & Structural Dynamics*. 42 (2), 297–310.

[18] Bozorgnia, Y., Abrahamson, N.A., Al Atik, L., Ancheta, T.D., Atkinson, G.M., Baker, J.W., et al. (2014) NGA-West2 research project. *Earthquake Spectra*. 30 (3), 973–987.

[19] Aagaard, B.T., Graves, R.W., Rodgers, A., Brocher, T.M., Simpson, R.W., Dreger, D., et al. (2010) Ground-motion modeling of hayward fault scenario earthquakes, part ii: Simulation of long-period and broadband ground motions. *Bulletin of the Seismological Society of America*. 100 (6), 2945–2977.

[20] Graves, R., Jordan, T.H., Callaghan, S., Deelman, E., Field, E., Juve, G., et al. (2011) CyberShake: A physics-based seismic hazard model for southern California. *Pure and Applied Geophysics*. 168 (3–4), 367–381.

[21] Moschetti, M.P., Hartzell, S., Ramírez-Guzmán, L., Frankel, A.D., Angster, S.J., and Stephenson, W.J. (2017) 3D ground-motion simulations of Mw 7 earthquakes on the salt lake city segment of the wasatch fault zone: Variability of long-period (T ≥ 1 s) ground motions and sensitivity to kinematic rupture parameters. *Bulletin of the Seismological Society of America*. 107 (4), 1704–1723.

[22] Wirth, E.A., Chang, S.W., and Frankel, A.D. (2018) 2018 report on incorporating sedimentary basin response into the design of tall buildings in Seattle, Washington: *Open-File Report 2018–1149*. United States Geological Survey, Reston, VA.

[23] Stephenson, W.J., Reitman, N.G., and Angster, S.J. (2017) P- and S-wave Velocity Models Incorporating the Cascadia Subduction Zone for 3D Earthquake Ground Motion Simulations, Version 1.6—Update for Open-File Report 2007–1348. *Open-File Report 2017-1152*. United States Geological Survey, Reston, VA.

[24] Marafi, N.A., Eberhard, M.O., Berman, J.W., Wirth, E.A., and Frankel, A.D. (2019) Impacts of simulated M9 cascadia subduction zone motions on idealized systems. *Earthquake Spectra*. 35 (3), 1261–1287.

[25] ACI (2014) 318-14: Building code requirements for structural concrete and commentary. American Concrete Institute, Farmington Hills, MI.

[26] PEER (2010) Modeling and acceptance criteria for seismic design and analysis of tall buildings PEER/ATC 72-1. Pacific Earthquake Engineering Research Center, University of California, Berkeley, CA.

[27] Jalayer, F. and Cornell, C.A. (2009) Alternative non-linear demand estimation methods for probability-based seismic assessments. *Earthquake Engineering & Structural Dynamics*. 38 (8), 951–972.

[28] USGS (2019) National Seismic Hazard Mapping Project (NSHMP) code, United States Geological Survey. Retrieved from www.usgs.gov.

[29] Jayaram, N., Lin, T., and Baker, J.W. (2011) A Computationally efficient ground-motion selection algorithm for matching a target response spectrum mean and variance. *Earthquake Spectra*. 27 (3), 797–815.

[30]   Hueste, M.B.D., Kang, T.H.K., and Robertson, I.N. (2009) Lateral drift limits for structural concrete slab-column connections, including shear reinforcement effects. *Proceedings, 2009 Structures Congress*. Austin, TX.

[31]   Hueste, M.B.D., Browning, J.A., Lepage, A., and Wallace, J.W. (2007) Seismic design criteria for slab-column connections. *ACI Structural Journal*. 104 (4), 448–458.

[32]   Dilger, W.G. and Cao, H. (1991) Behaviour of slab-column connections under reversed cyclic loading. Proceedings, 2nd International Conference of High-Rise Buildings. Beijing: Atlantis Press.

[33]   Dilger, W.G. and Brown, S.J. (1995) Earthquake resistance of slab-column connection. In Festschrift Professor Dr. Hugo Bachmann Zum, 22–27. ETH Zurich, Switzerland.

[34]   Megally, S. and Ghali, A. (2000) Punching shear design of earthquake-resistant slab column connections. *ACI Structural Journal*. 97 (5), 720–730.

[35]   Baker, J.W. (2015) Efficient analytical fragility function fitting using dynamic structural analysis. *Earthquake Spectra*. 31 (1), 579–599.

[36]   NEHRP (2011) Selecting and scaling earthquake ground motions for performing responsehistory analyses, NIST GCR 11-917-15 Prepared by NEHRP Consultants Joint Venture for the National Institute of Standards and Technology, Gaithersburg, MD.

[37]   Moehle, J. and Deierlein, G.G. (2004) A framework methodology for Performance-Based Earthquake Engineering. *Proceedings, 13th World Conference on Earthquake Engineering*. Vancouver, BC, Canada.

[38]   FEMA (2012) Seismic Performance Assessment of Buildings FEMA P-58, Federal Emergency Management Agency, Washington, DC.

[39]   SP3 (2019) Seismic Performance Prediction Program [Computer Software], Haselton Baker Risk Group, Chico, CA.

[40]   RS Means (2019) Building construction cost data R.S. Means Company, Kingston, MA.

[41]   USGS (2018) The HayWired earthquake scenario. Engineering implications, United States Geological Survey Scientific Investigations Report 2017-5013-I-Q, Reston, VA.

[42]   ATC (2018) San Francisco Tall Buildings Study, Applied Technology Council, Redwood City, CA.

[43]   Kourehpaz, P., Molina Hutt, C., Marafi, N.A., Berman, J.W., and Eberhard, M.O. (2020) Estimating economic losses of mid-rise RC wall residential buildings in sedimentary basins by combining empirical and simulated seismic hazard characterizations. *In-Preparation*.

[44]   Ramirez, C.M. and Miranda, E. (2012) Significance of residual drifts in building earthquake loss estimation. *Earthquake Engineering and Structural Dynamics*. 41 (11), 1477–1493.